Cell-Free and User-Centric Massive MIMO Architectures for Reliable Communications in Indoor Factory Environments

Mario Alonzo, Paolo Baracca, Saeed R. Khosravirad, and Stefano Buzzi

Factory automation is one of the use cases for 5G-and-beyond mobile networks where strict requirements in terms of latency, availability and reliability are required. In this paper, we investigate the potentials of massive MIMO in delivering those promises for industrial automation. Namely, communications between actuators (ACs) and Access Points (APs) inside an industrial scenario is considered and different transmission modes are compared: joint transmission (JT) where the distributed antennas are used to communicate with each AC, cell-free transmission (CFT) where all the ACs are served by all APs, single AP transmission (SAT) where each AC is served by only one AP, and user-centric transmission (UCT) where each AC is served by a subset of APs. A power control strategy, aimed at maximizing the minimum signal-to-interference plus noise ratio (SINR), is also introduced. Numerical results, shown in terms of downlink SINR and achievable rate, evaluated using the final block length capacity formula (FBLC), demonstrate that the use of distributed antenna setting and of power control bring substantial performance improvements in terms of reliability and latency.

***Index Terms*—Distributed MIMO, cell-free massive MIMO, user-centric approach, microwave, signal-to-interference plus noise ratio, power control, wireless networks, factory automation.**

I. Introduction

In the recent past, the use of wireless communications in factory automation has attracted a lot of interest in the scientific community [1]–[4]. Indeed, using wireless links permits avoiding the installation and maintenance of the network cables, providing increased robusteness and greater flexibility. Wireless factory automation is thus one of the most important use-cases of the fifth-generation (5G) of mobile networks [2]. 5G systems have to satisfy a wide set of stringent requirements, such as low latency, high reliability, and availability. This has led to the concept of ultra reliable and low latency communications (URLLC) [5], [6], which are instrumental to the development of new applications such as autonomous driving, remote control of drones, and wireless control of actuators (ACs) in factories. To this end, the 3rd Generation Partnership Project (3GPP) has already defined different indoor industrial scenarios, with strict requirements on the latency [7], and several research groups worldwide are addressing the design of URLLC systems. Paper [8] addresses the analysis in terms of coverage and capacity for different strategies, wherein a frequency planning is used to enhance the system performances. The work [9] has shown that in industrial scenarios, with focus on URLLC and on traffic analysis, network slicing can be a good strategy to satisfy different requirements given by both low-latency and high data rates. In [10] it has been demonstrated that, in industrial applications, under suitable hypotheses such as the deterministic traffic pattern, it is possible to shorten the size of OFDM preamble to reduce the latency, by adopting techniques for packet detection of OFDM signals. The work [11] addressed the problem of resource allocation of short packet transmission for factory scenarios by comparing four different transmission schemes, orthogonal multiple access (OMA), non-orthogonal multiple access (NOMA), relay-assisted transmission and cooperative NOMA (C-NOMA) transmission. Under suitable constraints, the authors described an optimization problem aimed to jointly optimizing the blocklength and power allocation to minimize the decoding error probability. Paper [12] considered a scenario wherein the access points (APs) form a distributed multiantenna system, to communicate with the active ACs in the factory, assuming that the small scale fading was modelled as the common Rayleigh fading, instead, a path-loss model for industrial scenario was used [13]. The performances in term of SINR, for different deployments, different beamforming, in case of equal and optimal power allocation [14] was analyzed. In [15], the authors analyse the Distributed MIMO (D-MIMO) systems for industrial scenarios, by exploiting a more realistic 3GPP compliant spatial channel model [16], taking into account the small scale fading model in conjunction with a path-loss model defined in [13]. It is shown in the paper that by using a distributed multiantenna architecture it is possible to improve the network reliability. In particular, the authors addressed the problem of Link Adaptation (LA), considering the block error rate (BLER) as KPI and evaluating different transmission modes, beamformers, with varying number of APs and ACs. That paper focused the attention to a target BLER of 10^{-5}, which is an extremely low value, required in the URLLC.

In this work, we study transmission modes in a distributed antenna setting for industrial scenarios. We build upon a recently proposed network architecture concept, dubbed cell-free (CF) networks. [17]. In CF, all the APs serve all the ACs, and all the APs are connected through a backhaul link to a central processing units (CPU), but every AP performs channel estimation locally, and the channel estimates are not shared

The work of M. Alonzo and S. Buzzi was supported by the MIUR program "Dipartimenti di Eccellenza 2018-2022".

This paper was partly presented at 24th International ITG Workshop on Smart Antennas, Hamburg (Germany), February 2020 and at the 2019 IEEE 90th Vehicular Technology Conference, Honolulu (USA), September 2019.

M. Alonzo and S. Buzzi are with *University of Cassino and Southern Latium*, Cassino, Italy, {mario.alonzo, buzzi}@unicas.it; they are also with *Consorzio Nazionale Interuniversitario per le Telecomunicazioni (CNIT)*, Parma, Italy.

P. Baracca is with *Nokia Bell Labs*, Stuttgart, Germany, paolo.baracca@nokia-bell-labs.com.

S. R. Khosravirad is with *Nokia Bell Labs*, Murray Hill, United States, saeed.khosravirad@nokia-bell-labs.com.

among APs. Moreover, the beamformers are locally evaluated, which leads to a limited usage of the backhaul link. During the downlink data transmission, the CPU sends the data symbols to the APs to be then forwarded to all ACs. In addition to CF, it is possible to derive the user-centric (UC), similarly to [18], wherein each AC, based on an association rule, has to choose the APs to connect to; this approach permits to reduce the amount of data to be sent through the backhaul link. In case of conjugate beamforming, a lower bound for the signal-to-interference-plus-noise ratio (SINR) can be evaluated in a closed form, as discussed in [17]. Moreover, a rate analysis will be addressed, by using the recent FBLC formula [19], which takes into account the length of the codewords and a target error. The problem of power control is also addressed, in order to maximize the minimum SINR across users; this is extremely important when reliability is more critical than data rates. The Time Division Duplex (TDD) protocol is considered, in order to exploit the reciprocity of the channel.

The paper is organized as follows. Section II contains the system model, while Section III is devoted to the description of transceiver processing. The adopted performance measures, i.e. the SINR and the finite blocklength rate, are illustrated in Section IV, while Section V contains the discussion of the power control rule. Numerical results are discussed in Section VI, while, finally, concluding remarks are reported in Section VII.

Notation. We use $(\cdot)^T$ and $(\cdot)^H$ to denote transpose and conjugate transpose, respectively. $\|\mathbf{X}\|$ is the norm of $\mathbf{X}$, $\mathbf{X}_{:,n}$ indicates the n-th column of matrix $\mathbf{X}$.

II. System model

An industrial scenario represented by an indoor factory hall is considered. We denote by K the total number of ACs equipped with a single antenna element, by J the number of APs distributed in the factory hall, and by M_{TOT} the total number of antenna elements, thus implying that $M = M_{TOT}/J$ is the number of antennas for each AP.

We consider the cases of

a) *centralized deployment*[1], where a single AP equipped with M_{TOT} antennas is placed at the center of the factory hall, so that the communication infrastructure resembles a single-cell network;
b) *distributed deployment*, where J APs equipped with M antennas each are placed in the factory hall; in this situation the communication infrastructure resembles a multi-cell network. The APs are assumed to be connected to a central processing unit (CPU) through reliable links.

We denote by $\mathbf{h}_{k,j}$ the $(M \times 1)$-dimensional uplink channel vector between the k-th AC and the j-th AP[2], defined as:

$$\mathbf{h}_{k,j} = \sqrt{\beta_{k,j}}\mathbf{f}_{k,j} \ , \tag{1}$$

where $\beta_{k,j}$ represents the large scale fading, i.e. path-loss plus shadowing, while $\mathbf{f}_{k,j}$ is the small scale fading vector, whose entries are a sequence of i.i.d. $\mathcal{CN}(0,1)$ random variables. Since the time division duplex protocol is used, we have channel reciprocity and the downlink channel between the j-th AP and the k-th AC is expressed as $\mathbf{h}_{k,j}^H$.

A. Transmission modes

Four different transmission modes to serve the ACs are considered in this paper.

1) *Joint Transmission (JT)*. All the APs serve all the ACs by using the same time-frequency resource. In this case, the system is equivalent to a network with a single AP having distributed antennas. All the computations of the downlink beamformers are done by the CPU.
2) *Single AP Transmission (SAT)*. Each AC k is served only by one AP, whose index is denoted by j_k. A reasonable choice is to let every AC to be served by the AP with the strongest large scale fading coefficient, i.e.

$$j_k = \underset{j=1,2,\ldots,J}{\arg\max}\, \beta_{k,j} \ , \ \ k = 1, \ldots, K \, . \tag{2}$$

SAT mode resembles a traditional wireless cellular network where each mobile device is linked to one base station at a time.
3) *Cell-Free Transmission (CFT)*. Following the transmission scheme developed in [17], [20], in this case all the APs serve all the users, similar to the JT case, but the channel estimates computed at the APs are not shared by the CPU and, instead, the beamformers are computed locally. The CFT is thus a simplified version of the JT with less deployment complexity.
4) *User-Centric Transmission (UCT)*. Following the scheme proposed in [21], this transmission mode resembles the CFT, with the difference that now every AC is served by a certain subset of APs. Although several AC-AP association rules can be conceived, in this paper we will restrict our attention to the case in which every AC is served by a certain number, say N, with $N \leq J$, of APs. A possible strategy may be to let the k-th AC to be served by the N APs that have the strongest large scale fading coefficients. Otherwise stated, letting $j_k(1), j_k(2), \ldots, j_k(J)$ a sequence of indexes such that $\beta_{k,j_k(1)} \geq \beta_{k,j_k(2)}, \geq \ \ldots \ \geq \beta_{k,j_k(J)}$, in the UCT mode the k-th AC is served by the APs with indexes $j_k(1), j_k(2), \ldots, j_k(N)$. We will denote by $\mathcal{J}(k)$ the set of APs serving the k-th AC. Similarly, $\mathcal{K}(j)$ will denote the set of ACs served by the j-th AP. Clearly, if $\widetilde{j} \in \mathcal{J}(\widetilde{k})$, then we have $\widetilde{k} \in \mathcal{K}(\widetilde{j})$.

It is worth noting that in a centralized deployment (i.e. $J = 1$) all the above transmission modes end up coincident. Additionally, it is useful to realize that the transmission modes SAT, CFT and UCT can be treated in an unified way, since they can be obtained through a proper definition of the sets $\{\mathcal{J}(k)\}_{k=1}^K$; in particular, we have that SAT corresponds to the choice $\mathcal{J}(k) = \{j_k(1)\}$; CFT corresponds to the choice $\mathcal{J}(k) = \{1, \ldots, J\}$; and, finally, UCT for a given N corresponds to the choice $\mathcal{J}(k) = \{j_k(1), j_k(2), \ldots, j_k(N)\}$. Finally, as regards the load on the backhaul link in distributed

[1]This deployment is considered as a benchmark to enable comparison with distributed deployments.

[2]For the case of centralized deployment there will be just one channel vector, $\mathbf{h}_{k,1}$, for any $k = 1, \ldots, K$.

deployments, it is easy to realize that JT poses the largest load on the backhaul, followed in decreasing order by CFT, UCT, and SAT.

III. Transceiver processing

We now describe the needed transceiver processing for the above mentioned transmission modes and deployment strategies.

A. Uplink training

Regardless of the transmission mode and of the deployment strategy, during the uplink training the ACs transmit pilot sequences in order to enable channel estimation at the APs. Let T be the length (in discrete-time samples) of the training sequences. We define by $\mathbf{\Phi} \in \mathcal{C}^{T\times K}$ the matrix containing on its k-th column the pilot sequence sent by the k-th AC. We assume that this matrix has orthogonal columns, with unitary norm. The received signal, $\mathbf{Y}_j$, at the j-th AP is an $M \times T$-dimensional matrix, written as:

$$\mathbf{Y}_j = \sum_{k=1}^{K} \sqrt{\eta_k^{UL-T}} \mathbf{h}_{k,j} \mathbf{\Phi}_{:,k}^H + \mathbf{W}_j \ . \tag{3}$$

In the above equation, $\eta_k^{UL-T} = \tilde{\eta}_k^{UL-T}\ T$ is the transmitted power by the k-th AC, $\mathbf{\Phi}_{:,k}$ is the k-th column of $\mathbf{\Phi}$, $\mathbf{W}_j$ is the $M \times T$-dimensional matrix of thermal noise samples, whose entries are assumed to be i.i.d. $\mathcal{CN}(0, \sigma_w^2)$ random variables. Based on the observable (3) at the j-th AP, in order to estimate the channel from the k-th AC $\mathbf{h}_{k,j}$, a projection onto the k-th pilot sequence is done:

$$\begin{aligned}\check{\mathbf{y}}_{k,j} = \mathbf{Y}_j \mathbf{\Phi}_{:,k} = \ & \sqrt{\eta_k^{UL-T}} \mathbf{h}_{k,j} + \\ & \sum_{l=1,l\neq k}^{K} \sqrt{\eta_l^{UL-T}} \mathbf{h}_{l,j} \mathbf{\Phi}_{:,l}^H \mathbf{\Phi}_{:,k} + \mathbf{W}_j \mathbf{\Phi}_{:,k} \ .\end{aligned} \tag{4}$$

Given the M-dimensional vector $\check{\mathbf{y}}_{k,j}$, and, assuming that the large scale fading coefficients are known at the APs, a linear minimum mean square error (LMMSE) estimate for the channel vector $\mathbf{h}_{k,j}$ is obtained as follows:

$$\hat{\mathbf{h}}_{k,j} = \underbrace{\frac{\sqrt{\eta_k^{UL-T}}\beta_{k,j}}{\sum_{l=1}^{K} \eta_l^{UL-T}\beta_{l,j} \mid \mathbf{\Phi}_{:,l}^H \mathbf{\Phi}_{:,k} \mid^2 + \sigma_w^2}}_{\alpha_{k,j}} \check{\mathbf{y}}_{k,j}. \tag{5}$$

Some remarks are now in order. First of all, other channel estimation strategies can be pursued; in this paper, we consider LMMSE estimation due to its simplicity and optimality among linear estimation rules. Next, notice that channel estimation is performed locally at each AP. For CFT and UCT and SAT, this information is exploited locally for computing the beamformer; for the case of JT, instead, these estimates are to be sent to the CPU.

B. Downlink transmission and beamforming criteria

Let us detail now the transmitted signal model. Denoting by $x_k(n)$ the unit-energy information symbol to be sent to the k-th AC in the n-th symbol interval, and by $\eta_{k,j}$ and $\mathbf{q}_{k,j}$ the transmit power and the M-dimensional transmit beamformer used at the j-th AP to transmit to the k-th AC, respectively, the signal transmitted by the j-th AP for SAT, CFT and UCT can be generally expressed as

$$\mathbf{s}_j(n) = \sum_{k\in\mathcal{K}(j)} \sqrt{\eta_{k,j}} \mathbf{q}_{k,j} x_k(n) \ . \tag{6}$$

The signal received by the k-th AC can be easily shown to be expressed as

$$\begin{aligned}\hat{x}_k(n) &= \sum_{j=1}^{J} \mathbf{h}_{k,j}^H \mathbf{s}_j(n) + z_k(n) \\ &= \sum_{j\in\mathcal{J}(k)} \sqrt{\eta_{k,j}} \mathbf{h}_{k,j}^H \mathbf{q}_{k,j} x_k(n) + \\ &\quad \sum_{l=1,l\neq k}^{K} \sum_{j\in\mathcal{J}(l)} \sqrt{\eta_{l,j}} \mathbf{h}_{k,j}^H \mathbf{q}_{l,j} x_l(n) + z_k(n),\end{aligned} \tag{7}$$

where $z_k(n)$ is the additive thermal noise distributed as $\mathcal{CN}(0, \sigma^2)$.

For the case of JT, instead, denoting by η_k the overall power used to transmit to AC k, the M-dimensional vector transmitted by the j-th AP in the n-th interval is written as

$$\mathbf{s}_j(n) = \sum_{k=1}^{K} \sqrt{\eta_k} \mathbf{q}_{k,j} x_k(n) \ . \tag{8}$$

Upon letting $\mathbf{q}_k = [\mathbf{q}_{k,1}^T, \mathbf{q}_{k,2}^T, \ldots, \mathbf{q}_{k,J}^T]^T$ and $\mathbf{h}_k = [\mathbf{h}_{k,1}^T, \mathbf{h}_{k,2}^T, \ldots, \mathbf{h}_{k,J}^T]^T$ denote the M_{TOT}-dimensional overall beamformer and channel vector for AC k, the signal received at the k-th AC can be shown to be written as

$$\hat{x}_k(n) = \eta_k \mathbf{h}_k^H \mathbf{q}_k x_k(n) + \sum_{l=1,l\neq k}^{K} \eta_l \mathbf{h}_k^H \mathbf{q}_l x_l(n) + z_k(n) \ . \tag{9}$$

Deferring to the next section the discussion about the used power control rules, we focus now on the problem of beamforming design. Several beamformers will be considered here.

1) Maximum ratio transmission (MRT)

The MRT beamformer (a.k.a. channel matched beamformer) is simply defined as $\mathbf{q}_k^{(MRT)} = \hat{\mathbf{h}}_k / \|\hat{\mathbf{h}}_k\|$, for JT mode, and as $\mathbf{q}_{k,j}^{(MRT)} = \hat{\mathbf{h}}_{k,j} / \|\hat{\mathbf{h}}_{k,j}\|$, for SAT, CFT, and UCT modes.

2) Full zero forcing (FZF)

Zero-forcing strategies tend to nullify the interference contribution through projection along suitable signal subspaces. For the case of JT, interference cancellation can take place only if $K \leq M_{TOT}$. Under this assumption, letting $\hat{\mathbf{H}} = [\hat{\mathbf{h}}_1, \ldots, \hat{\mathbf{h}}_K]^H$ be the $(K \times M_{TOT})$-dimensional whole estimated channel matrix, and defining $\mathbf{Q} = \hat{\mathbf{H}}^H (\hat{\mathbf{H}}\hat{\mathbf{H}}^H)^{-1}$, the FZF beamformer to be used when transmitting to the k-th AC is written as: $\mathbf{q}_k^{(FZF)} = \mathbf{Q}_{:,k} / \|\mathbf{Q}_{:,k}\|$. This beamformer is computed by the CPU; then it is split into J parts with M entries each and sent to the APs.

Let us consider now the case of SAT, CFT and UCT modes. In this case, the zero-forcing projection is to be done on M-dimensional vectors, so interference cancellation can be obtained only if $K \leq M$. Under this assumption, letting $\hat{\mathbf{H}}_j = [\hat{\mathbf{h}}_{1,j}, \ldots, \hat{\mathbf{h}}_{K,j}]^H$ be the $(K \times M)$-dimensional whole estimated channel matrix at AP j, and defining $\mathbf{Q}_j = \hat{\mathbf{H}}_j^H (\hat{\mathbf{H}}_j \hat{\mathbf{H}}_j^H)^{-1}$, the FZF beamformer to be used at the j-th AP when transmitting to the k-th AC is written as $\mathbf{q}_{k,j}^{(FZF)} = \mathbf{Q}_{j\,:,k} / \|\mathbf{Q}_{j\,:,k}\|$.

3) Partial zero forcing (PZF)

As discussed above, FZF beamforming is capable of nullifying the interference only if the number of ACs is not larger than the number of antennas at the APs. Moreover, when the number of ACs approaches the number of antennas at the AP, the performance starts degrading due to the well-known noise enhancement effect [22]. In order to avoid this effect, a compromise solution may be to adopt a PZF beamformer, wherein every AP nulls the interference only to a subset of the ACs in the system. A reasonable choice is to nullify the interference only towards the ACs to which the greatest harm is produced. In particular, with reference to SAT, CFT and UCT modes, assuming that the k-th AC is served by the j-th AP (i.e., $k \in \mathcal{K}(j)$), let us denote by $N_j < M$, the number of ACs to be protected from the interference generated by the AP j when transmitting to the k-th AC. The PZF beamformer for AP j and AC k can be then obtained as follows. Consider the set $\{\beta_{1,j}, \beta_{2,j}, \ldots, \beta_{K,j}\} - \{\beta_{k,j}\}$ containing $K-1$ coefficients and let $k_j(1), k_j(2), \ldots, k_j(K-1)$ be a sequence of indexes such the $K-1$ coefficients of the set are ordered in decreasing order. Build the $((N_j+1) \times M)$-dimensional matrix $\mathbf{H}_{k,j} = [\hat{\mathbf{h}}_{k,j}, \hat{\mathbf{h}}_{k_j(1),j}, \hat{\mathbf{h}}_{k_j(2),j}, \ldots \hat{\mathbf{h}}_{k_j(N_j),j}]^H$. Define the matrix $\mathbf{Q}_{k,j} = \hat{\mathbf{H}}_{k,j}^H (\hat{\mathbf{H}}_{k,j} \hat{\mathbf{H}}_{k,j}^H)^{-1}$; the PZF beamformer is finally obtained as: $\mathbf{q}_{k,j} = [\mathbf{Q}_{k,j}]_{:,1} / \|[\mathbf{Q}_{k,j}]_{:,1}\|$.

The PZF beamformer for JT mode can be obtained through similar steps. We omit the details for the sake of brevity.

IV. Performance measures

As performance measures we consider the downlink SINR and the achievable rate under the FBLC [19].

A. SINR expressions for SAT, CFT and UCT modes

Given (7), it is easy to realize that an upper bound for SINR of the k-th user follows as:

$$\text{SINR}_k^{UB} = \frac{\left| \sum_{j \in \mathcal{J}(k)} \sqrt{\eta_{k,j}} \mathbf{h}_{k,j}^H \mathbf{q}_{k,j} \right|^2}{\sigma_k^2 + \sum_{l=1, l \neq k} \left| \sum_{j \in \mathcal{J}(l)} \sqrt{\eta_{l,j}} \mathbf{h}_{k,j}^H \mathbf{q}_{l,j} \right|^2}. \quad (10)$$

The superscript UB stands for upper-bound. We remark that the UB expression (10) holds for any of the above described beamformers. Since (10) depends on the true channel realizations, using it into the Shannon rate formula $B \log(1+\text{SINR})$, with B the communication bandwidth, leads to a rate that is an upper bound of the achievable rate [23]. This bound becomes tight when the channel state information accuracy improves, and for perfect channel knowledge it provides the exact value of the achievable rate.

In practical scenarios, however, where channel estimation errors occur, using the SINR expression in (10) for computing the achievable rate leads to optimistic results that are not useful for conservative system design. To circumvent this problem, a bounding technique, known as the "use and then forget" bound [23, Chapter 2], can be used, which leads to a lower bound on SINR that when plugged in the Shannon's achievable rate formula provides a lower bound for the achievable rate. Assuming that each AC has the knowledge of the channel statistics, starting from (7), we can write:

$$\begin{aligned} \hat{x}_k = & \underbrace{\mathbb{E}\left[\sum_{j \in J(k)} \sqrt{\eta_{k,j}} \mathbf{h}_{k,j}^H \mathbf{q}_{k,j} \right]}_{D_k} x_k^{DL} + \\ & \underbrace{\left(\sum_{j \in J(k)} \sqrt{\eta_{k,j}} \mathbf{h}_{k,j}^H \mathbf{q}_{k,j} - \mathbb{E}\left[\sum_{j \in J(k)} \sqrt{\eta_{k,j}} \mathbf{h}_{k,j}^H \mathbf{q}_{k,j} \right] \right)}_{B_k} x_k^{DL} + \\ & + \sum_{l \neq k} \underbrace{\sum_{j \in J(l)} \sqrt{\eta_{k,j}} \mathbf{h}_{k,j}^H \mathbf{q}_{l,j}}_{I_{k,l}} x_l^{DL} + z_k \end{aligned} \quad (11)$$

where D_k, B_k, and $I_{k,j}$ represent the strength of desired signal, the beamforming gain uncertainty, and the interference caused by the transmission to the l-th AC, respectively. A lower bound to the SINR for the k-th AC can be thus written as:

$$\text{SINR}_k^{LB} = \frac{|D_k|^2}{\mathbb{E}\left[|B_k|^2\right] + \sum_{l=1, l \neq k}^{K} \mathbb{E}\left[|I_{k,l}|^2\right] + \sigma_k^2} \quad (12)$$

The lower bound (12) holds for any beamformer. Closed form expressions for the SINR (12) can be obtained for the case of generalized MRT beamforming, i.e. for $\mathbf{q}_{k,j}^{(MRT)} = \hat{\mathbf{h}}_{k,j} / \|\hat{\mathbf{h}}_{k,j}\|^\lambda$, with $\lambda \in \{0, 1, 2\}$ the normalization exponent [24], [25].

For the case in which $\lambda = 0$, i.e. a non-normalized MRT is employed, letting $\gamma_{k,j} = \sqrt{\eta_k^{UL-T}} \beta_{k,j} \alpha_{k,j} M$, the SINR lower bound can be shown to be expressed as in (13), shown at the top of next page. The proof of expression (13) is reported in Appendix A. Given the fact that non-normalized MRT beamformers are used, the total average power transmitted by AP j is now expressed as

$$P_j = \sum_{k \in \mathcal{K}(j)} \eta_{k,j} \gamma_{k,j}. \quad (14)$$

B. SINR expressions for JT mode

Given expression (9), and following similar steps as in the previous section, an upper bound for the SINR can be written as:

$$\text{SINR}_k^{UB} = \frac{\eta_k \mid \mathbf{h}_k^H \mathbf{q}_k \mid^2}{\sigma_k^2 + \sum_{l=1, l \neq k}^{K} \eta_l \mid \mathbf{h}_k^H \mathbf{q}_l \mid^2}, \quad (15)$$

where σ_k^2 is the thermal noise variance.

This article has been accepted for publication in a future issue of this journal, but has not been fully edited. Content may change prior to final publication. Citation information: DOI 10.1109/OJCOMS.2021.3089281, IEEE Open Journal of the Communications Society

$$\text{SINR}_k^{LB} = \frac{\left(\sum\limits_{j\in J(k)} \sqrt{\eta_{k,j}}\gamma_{k,j}\right)^2}{\sum\limits_{l=1}^{K}\sum\limits_{j\in J(l)} \eta_{l,j}\beta_{k,j}\gamma_{l,j} + \sum\limits_{l=1,l\neq k}^{K}\left(\sum\limits_{j\in J(l)} \sqrt{\eta_{l,j}}\frac{\sqrt{\eta_k^{UL-T}}}{\sqrt{\eta_l^{UL-T}}}\frac{\beta_{k,j}}{\beta_{l,j}}\gamma_{l,j}\right)^2 \left|\mathbf{\Phi}_{:,k}^H\mathbf{\Phi}_{:,l}\right|^2 + \sigma_k^2} \,. \tag{13}$$

Similarly, a lower bound can be also derived through the "use and then forget" bound. Indeed, starting from (9), we have:

$$\hat{x}_k = \eta_k(\underbrace{\mathbb{E}[\mathbf{h}_k^H\mathbf{q}_k]}_{D_k})x_k^{DL} + \eta_k(\underbrace{\mathbf{h}_k^H\mathbf{q}_k - \mathbb{E}[\mathbf{h}_k^H\mathbf{q}_k]}_{B_k})x_k^{DL} + \sum_{l\neq k}\eta_l\underbrace{\mathbf{h}_k^H\mathbf{q}_l}_{I_{k,l}}x_l^{DL} + z_k \,, \tag{16}$$

which leads to the following expression

$$\text{SINR}_k^{LB} = \frac{\eta_k|D_k|^2}{\eta_k\mathbb{E}\left[|B_k|^2\right] + \sum\limits_{l=1,l\neq k}^{K}\eta_l\mathbb{E}\left[|I_{k,l}|^2\right] + \sigma_k^2} \,. \tag{17}$$

Expression (17) can be given a closed-form expression for the case of generalized MRT beamforming, i.e. for $\mathbf{q}_k^{(MRT)} = \hat{\mathbf{h}}_k/\|\hat{\mathbf{h}}_k\|^\lambda$, with, again, $\lambda \in \{0,1,2\}$ the normalization exponent [24], [25].

For the case in which $\lambda = 0$, i.e. a non-normalized MRT is employed, as detailed in Appendix B, we have (18), at the top of next page. where $\mathbf{D}_k = \text{blkdiag}\left(\alpha_{k,1}\mathbf{I}_M, \alpha_{k,2}\mathbf{I}_M, \ldots \alpha_{k,J}\mathbf{I}_M\right)$ and $\mathbf{B}_k = \text{blkdiag}\left(\beta_{k,1}\mathbf{I}_M, \beta_{k,2}\mathbf{I}_M, \ldots \beta_{k,J}\mathbf{I}_M\right)$. The total average transmitted power is now expressed as $\sum\limits_{l=1}^{K}\eta_l\gamma_l$.

C. Finite Block Length Capacity

The SINR expression derived above can be used to compute upper and lower bounds to the achievable rate. Traditionally, the rate expression is written as $\text{R}_k = B\,\log_2(1+\text{SINR}_k)$ where B is the bandwidth, but this formula holds for asymptotically long Gaussian distributed codewords. When strict latency constraints need to be met, as usually happens in the case of remote machine control, coding schemes with short codewords are used and the traditional rate formula does not hold any longer. In [19], the FBLC formula was derived; in particular, letting m be the length in symbols of the used codeword and ϵ the target error probability, the k-th AC rate in the finite block length regime can be approximated as

$$\text{R}_k \approx B\left[\log_2(1+\text{SINR}_k) - \sqrt{\frac{(1+\text{SINR}_k)^2-1}{m(1+\text{SINR}_k)^2}}\frac{\text{Q}^{-1}(\epsilon)}{\ln(2)}\right], \tag{19}$$

with $\text{Q}^{-1}(\cdot)$ denoting the inverse Q-function. Inspecting (19), it is readily seen that R_k is negative for small values of the SINR[3]. To better understand such behaviour, it is possible to consider the Taylor expansion of R_k with starting point $\text{SINR}_k = 0$. Letting $x_k = \text{SINR}_k$, and taking $x_k \ll 1$, the following relations hold:

$$\log_2(1+x_k) \approx \frac{x_k}{\ln(2)} \,,$$

and

$$\sqrt{1-\frac{1}{(1+x_k)^2}} \approx \sqrt{2}\sqrt{x_k} \,.$$

Then, for small x_k, R_k can be approximated as:

$$\text{R}_k \approx \frac{B}{\ln(2)}\left[x_k - \sqrt{\frac{2}{m}}\text{Q}^{-1}(\epsilon)\sqrt{x_k}\right] \tag{20}$$

It is easily seen from the above equation that $\text{R}_k = 0$ for $x_k = 0$ and that the first order derivative at $x_k = 0$ is negative; the rate R_k thus departs from the zero value of the SINR with a negative slope. This provides further evidence that the finite blocklength capacity takes negative values for small values of the SINR. It is also easily seen that this effect disappears as m grows, i.e. we approach the case of infinitely long codewords. Fig.1 shows the spectral efficiency for the case of asymptotically long Gaussian distributed codewords, and then shows the same spectral efficiency in the finite block length regime (assuming $\epsilon = 10^{-5}$ and $m = 100$), along with its first order approximation (20). It is clearly seen that there is an excellent agreement between the exact value of R_k and its first-order approximation for small values of the SINR. Moreover, as expected, the finite blocklength spectral efficiency is smaller than the classical Shannon expression of the spectral efficiency.

V. Power control strategies

A. Uniform power allocation

The simplest form of power control is the uniform power allocation (UPA), wherein each AP uniformly splits its available power budget across the ACs it is connected to. Denoting by $P_{\max,j}$ the maximum power available at AP j, the power coefficients $\eta_{k,j}$ are expressed as

$$\eta_{k,j} = \begin{cases} \frac{P_{\max,j}}{|\mathcal{K}(j)|} & k \in \mathcal{K}(j), \\ 0 & k \notin \mathcal{K}(j), \end{cases} \tag{21}$$

for the case of SAT, CFT and UCT modes with normalized beamformers. If, instead, a non-normalized MRT beamformer is used, then we have:

$$\eta_{k,j} = \begin{cases} \frac{P_{\max,j}}{|\mathcal{K}(j)|\gamma_{k,j}} & k \in \mathcal{K}(j), \\ 0 & k \notin \mathcal{K}(j) \,. \end{cases} \tag{22}$$

For the case of JT, denoting by $P_{\max}$ the maximum available power, and assuming that normalized beamformers are used, we simply have $\eta_k = P_{\max}/K$, $\forall k = 1,2,\ldots,K$. When a non-normalized MRT beamformer is used, we have instead $\eta_k = \frac{P_{\max}}{K\gamma_k}$.

[3]In this negative area the FBLC is clearly approximated with a zero value.

This article has been accepted for publication in a future issue of this journal, but has not been fully edited. Content may change prior to final publication. Citation information: DOI 10.1109/OJCOMS.2021.3089281, IEEE Open Journal of the Communications Society

$$\text{SINR}_k^{LB} = \frac{\eta_k \gamma_k^2}{\sum\limits_{l=1}^{K} \eta_l \sqrt{\eta_l^{UL-T}} \text{tr}(\mathbf{B}_l \mathbf{D}_l^H \mathbf{B}_k) + \sum\limits_{l=1, l\neq k}^{K} \eta_l \eta_k^{UL-T} \text{tr}^2(\mathbf{D}_l \mathbf{B}_k) |\mathbf{\Phi}_{:,k}^H \mathbf{\Phi}_{:,l}|^2 + \sigma_k^2}, \tag{18}$$

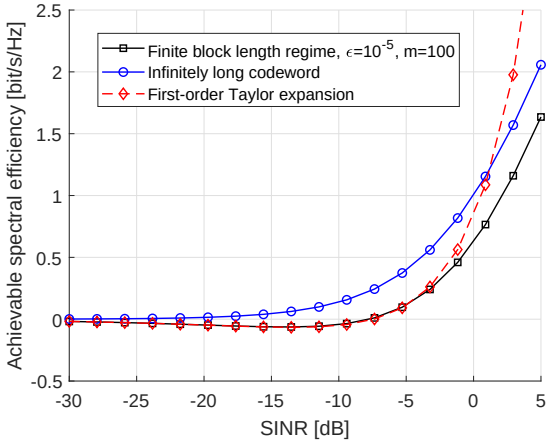

Figure 1: Plot, as a function of SINR, of the Shannon spectral efficiency, finite blocklength spectral efficiency, and of its first order expansion around the SINR value 0 (which is $-\infty$ in logarithmic units.).

B. Min-SINR maximum power allocation

Besides uniform power allocation, alternative power control strategies can be realized. As an example, transmit powers could be tuned to maximize the system sum-rate, or, also, the energy efficiency [26]. However, in an industrial wireless control setup it is important to provide a reliable wireless link to all ACs, thus making it crucial for the optimization framework to account for ACs with unfavorable channel. To this end, it may be helpful to allocate transmit power in order to maximize the minimum SINR across the K ACs. Notice that, since the achievable rate is an increasing function of the SINR[4], this strategy also maximizes the minimum of the ACs' rates.

1) SAT, CFT and UCT modes

For SAT, CFT, and UCT modes, the k-th AC SINR expression (13) can be written as

$$\text{SINR}_k = \frac{\left(\sum\limits_{j\in J(k)} \sqrt{\eta_{k,j}} a_{k,j} \right)^2}{\sum\limits_{l=1}^{K} \sum\limits_{j\in J(l)} \eta_{l,j} b_{l,j}^{(k)} + \sum\limits_{l=1, l\neq k}^{K} \left(\sum\limits_{j\in J(l)} \sqrt{\eta_{l,j}} c_{l,j}^{(k)} \right)^2 \varphi_{k,l} + \sigma_k^2}. \tag{23}$$

with suitable definitions of the coefficients $a_{k,j}$, $b_{l,j}^{(k)}$ and $c_{l,j}^{(k)}$, and $\varphi_{k,l} = \left| \mathbf{\Phi}_{:,k}^H \mathbf{\Phi}_{:,l} \right|^2$ The k-th AC SINR expression in (10) can be also represented as in (23) assuming $c_{l,j}^{(k)} = 0 \ \forall l, j, k$, and $b_{l,j}^{(k)} = 0$ when $l = k$. Let us focus for the moment on the SINR lower bound expression in (13). Letting $\mathcal{P} = \{\eta_{k,j} \ : \ j \in \mathcal{J}(k), \forall k = 1, \ldots, K\}$ be the set of unknown powers to be optimized, the problem (24), shown at the top of the next page, can be considered. Introducing the new variables $p_{k,j} \triangleq \sqrt{\eta_{k,j}}$, $\epsilon_{l,k} \triangleq \left(\sum\limits_{j\in J(l)} p_{l,j} c_{l,j}^{(k)} \right)^2$, and $\delta_j^{(k)} \triangleq \sum\limits_{l\in\mathcal{K}(j)} p_{l,j}^2 b_{l,j}^{(k)}$, and letting $\mathcal{Q} = \{\eta_{k,j} \ : \ j \in \mathcal{J}(k), \forall k = 1, \ldots, K\} \cup \left\{ \delta_j^{(k)} \ : \ j = 1, \ldots, J \right\} \cup \left\{ \epsilon_{l,k} \ : \ l, k \in \{1, \ldots, K\}^2, \ l \neq k \right\}$ the new set of variables to be optimized, problem (24) can be equivalently re-written as[5]

$$\begin{cases} \max\limits_{\mathcal{Q}} \min\limits_{k=1,\ldots,K} \dfrac{\left(\sum\limits_{j\in J(k)} p_{k,j} a_{k,j} \right)^2}{\sum\limits_{j=1}^{J} \delta_j^{(k)} + \sum\limits_{l=1, l\neq k}^{K} \epsilon_{l,k} \varphi_{k,l} + \sigma_k^2}, \\ \text{subject to:} \begin{cases} p_{k,j} \geq 0 \ , \ k = 1, \ldots, K \ \ j = 1, \ldots, J \ , \\ \sum\limits_{k\in\mathcal{K}(j)} p_{k,j}^2 \gamma_{k,j} \leq P_{\max,j} \ , \ j = 1, \ldots, J \ , \\ \left(\sum\limits_{j\in J(l)} p_{l,j} c_{l,j}^{(k)} \right)^2 \leq \epsilon_{l,k} \ , \forall l \neq k \ , \\ \sum\limits_{l\in\mathcal{K}(j)} p_{l,j}^2 b_{l,j}^{(k)} \leq \delta_j^{(k)} \ , \ j = 1, \ldots, J \ . \end{cases} \end{cases} \tag{25}$$

The objective function in (25) is quasi-concave. The proof of this result is omitted since it is already available in [17]. Accordingly, the optimal solution to (25) can be obtained by solving a sequence of convex feasibility programs, as detailed in Algorithm 1.

The case in which the SINR expression to be considered in the optimization problem is the upper bound (10) can be treated similarly, with the only difference that the maximum power constraint is now written as $\sum_{k\in\mathcal{K}(j)} p_{k,j}^2 \leq P_{\max,j}$. We omit the details for the sake of brevity.

2) JT mode

For the JT mode, it is seen that both the k-th AC SINR expressions (15) and (18) can be written as

$$\text{SINR}_k = \frac{\eta_k a_k}{\sum\limits_{j=1}^{K} \eta_j b_{k,j} + \sigma_k^2}, \qquad k = 1, \ldots, K \tag{27}$$

with suitable definitions for the coefficients $\{a_k\}_{k=1}^K$ and $\{b_{k,j}\}_{k,j=1}^K$. Letting $\eta = [\eta_1, \eta_2, \ldots, \eta_K]^T$ be the vector power

[4] As already discussed, this is also true for the rate expression in (19), provided that the negative values of the rates in the low SINR region are substituted by zero.

[5] Problem (25) is equivalent to (24) since at the optimal point the third and fourth constraints in (25) are satisfied with equality. The proof of this statement can be obtained by contradiction and is omitted for the sake of brevity.

This article has been accepted for publication in a future issue of this journal, but has not been fully edited. Content may change prior to final publication. Citation information: DOI 10.1109/OJCOMS.2021.3089281, IEEE Open Journal of the Communications Society

$$\begin{cases} \max\limits_{\mathcal{P}} \min\limits_{k=1,\ldots,K} \dfrac{\left(\sum\limits_{j\in J(k)} \sqrt{\eta_{k,j}} a_{k,j}\right)^2}{\sum\limits_{l=1}^{K} \sum\limits_{j\in J(l)} \eta_{l,j} b_{l,j}^{(k)} + \sum\limits_{l=1,l\neq k}^{K} \left(\sum\limits_{j\in J(l)} \sqrt{\eta_{l,j}} c_{l,j}^{(k)}\right)^2 \varphi_{k,l} + \sigma_k^2}, \\ \text{subject to:} \begin{cases} \eta_{k,j} \geq 0\ ,\ k=1,\ldots,K\ \ j=1,\ldots,J\ , \\ \sum\limits_{k\in\mathcal{K}(j)} \eta_{k,j}\gamma_{k,j} \leq P_{\max,j}\ ,\ j=1,\ldots,J\ . \end{cases} \end{cases} \tag{24}$$

Algorithm 1 Bisection algorithm for solving problem (24)

1: Choose $t_{\min}=0$ and $t_{\max}$ as a number certainly larger than the maximun SINR, e.g. $t_{\max}=10^8$. Choose a tolerance $\bar{\epsilon}>0$.
2: **while** $t_{\max}-t_{\min}>\bar{\epsilon}$ **do**
3: Set $t=\frac{t_{\max}+t_{\min}}{2}$
4: Solve the following convex feasibility program

$$\begin{aligned} &\|\mathbf{s}_k\| \leq \frac{1}{\sqrt{t}}\left(\sum_{j\in J(k)} p_{k,j} a_{k,j}\right), k=1,\ldots,K \\ &p_{k,j}\geq 0\ ,\ k=1,\ldots,K\ \ j=1,\ldots,J\ , \\ &\sum_{k\in\mathcal{K}(j)} p_{k,j}^2\gamma_{k,j} \leq P_{\max,j}\ ,\ j=1,\ldots,J\ , \\ &\left(\sum_{j\in J(l)} p_{l,j} c_{l,j}^{(k)}\right)^2 \leq \epsilon_{l,k}\ ,\forall l\neq k\ , \\ &\sum_{l\in\mathcal{K}(j)} p_{l,j}^2 b_{l,j}^{(k)} \leq \delta_j^{(k)}\ ,\ j=1,\ldots,J\ . \end{aligned} \tag{26}$$

5: **if** Problem (26) is feasible **then**
6: $t_{\min}=t$
7: **else**
8: $t_{\max}=t$
9: **end if**
10: **end while**

to be optimized, the problem at hand can be expressed as

$$\begin{cases} \max\limits_{\eta,t} t\ , \\ \text{subject to:} \begin{cases} \dfrac{\eta_k a_k}{\sum\limits_{j=1}^{K} \eta_j b_{k,j} + b_{0,k}} \geq t\ ,\ k=1,\ldots,K\ , \\ \eta_k > 0\ ,\ k=1,\ldots,K\ , \\ \sum\limits_{l=1}^{K} \eta_l \leq P_{\max}\ . \end{cases} \end{cases} \tag{28}$$

Problem (28) can be solved efficiently by a bisection search, in each step solving a sequence of convex feasibility problems [27] as detailed in Algorithm 2. In problem (28), the maximum power constraints $\sum_{l=1}^{K}\eta_l \leq P_{\max}$ refers to the case in which normalized beamformers are used; if, instead non-normalized MRT beamformers are employed, then the constraint becomes $\sum_{l=1}^{K}\eta_l\gamma_l \leq P_{\max}$.

With regard to the computational complexity of the proposed algorithms, it is worth underlining that we are dealing with convex feasibility programs, which can be efficiently solved in few iterations through off-the-shelf numerical routines. Given the fact that the quantities to optimize are just fraction of polynomials (for the JT mode even fraction of linear terms), the complexity of gradient-based methods is proportional to the number of variables to be optimized, which equals the number of ACs K times the average number of APs serving each AC.

Algorithm 2 Bisection algorithm for solving problem (28)

1: Choose $t_{\min}=0$ and $t_{\max}$ as a number certainly larger than the maximun SINR, e.g. $t_{\max}=10^8$. Choose a tolerance $\bar{\epsilon}>0$.
2: **while** $t_{\max}-t_{\min}>\bar{\epsilon}$ **do**
3: Set $t=\frac{t_{\max}+t_{\min}}{2}$
4: Solve the convex feasibility program (28)
5: **if** Problem (28) is feasible **then**
6: $t_{\min}=t$
7: **else**
8: $t_{\max}=t$
9: **end if**
10: **end while**

VI. Numerical Results

A. Simulation setup

We assume an industrial scenario with a factory hall of dimensions $100\times 50\times 6$ m^3; we consider a system bandwidth of 100 MHz at the carrier frequency of 3.7 GHz. We denote by $K=16$ the total number of ACs equipped with a single antenna element with height of 1.5 m, and by $M_{TOT}=64$ the total number of antennas to be subdivided among all the APs. The quantity J denotes the number of APs distributed in the factory hall and $M=M_{TOT}/J$ is the number of antennas for each AP. The APs are placed at a height of 6 meters[6]. In the following, numerical results are shown in terms of the CDF of the AC's SINR, and in terms of achievable rate-per-user versus the error probability. The latter curve has been obtained by fixing a value for the error probability ϵ and computing the average finite blocklength rate in (19) with $m=100$. We assume to use uniform power allocation from Fig. 3 up to Fig. 8 as it is our baseline. We focus our attention on the downlink (DL) transmission, and assume that the total transmit power is 20 dBm. We consider an additive white Gaussian

[6]We choose this value since it is the typical height in an indoor factory environment.

This article has been accepted for publication in a future issue of this journal, but has not been fully edited. Content may change prior to final publication. Citation information: DOI 10.1109/OJCOMS.2021.3089281, IEEE Open Journal of the Communications Society

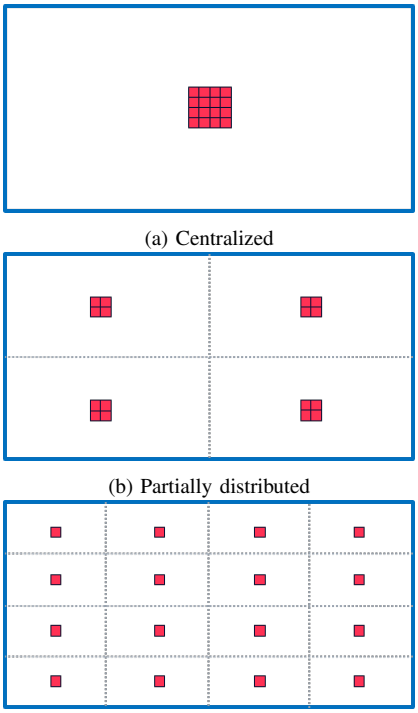

(a) Centralized

(b) Partially distributed

(c) Fully distributed

Figure 2: Considered AP deployments.

noise (AWGN) process with power spectral density of -174 dBm/Hz and a receiver noise figure (NF) of 7 dB.

B. Path-loss model

We adopt the 3GPP Indoor Office (InO) and Indoor Mixed (InM) channel models [16] and modify them based on the proposal in [13], where models for path-loss, shadowing, and line of sight (LOS) probability have been proposed based on extensive measurements done in two different operational factories at 3.5 GHz. Such novel Indoor Industrial (InI) model considers different deployments, distinguishing i) elevated (El) from clutter embedded (Cl) APs and ii) open (Op) from dense (De) production spaces, proposing for each configuration specific values of the aforementioned large scale fading parameters; all the details are reported in [13, Tab. 3].

First, we compare in Fig. 3 the InI models proposed in [13] against the InO and InM developed in 3GPP for indoor scenarios by showing the cumulative distribution function (CDF) of the SINR achieved by JT with $J = 16$ APs serving $K = 1$ AC with MRT and with perfect channel knowledge. We observe that the achieved SINR is quite large, as just one AC is active (i.e., there is no interference) on the whole factory floor, and a fully distributed deployment is used. However, there is significant difference among the different models, and it is seen that adopting the InI-Cl-De the value of the SINR CDF at 10^{-3} is almost 20 dB lower when compared to 3GPP's InO model. Based on such result, in the rest of the numerical results we consider the InI-Cl-De model as it represents the most challenging scenario. Further, we adopt the assumption of imperfect channel knowledge for beamforming design, as described in Section III-A, for pilot length $T = 16$.

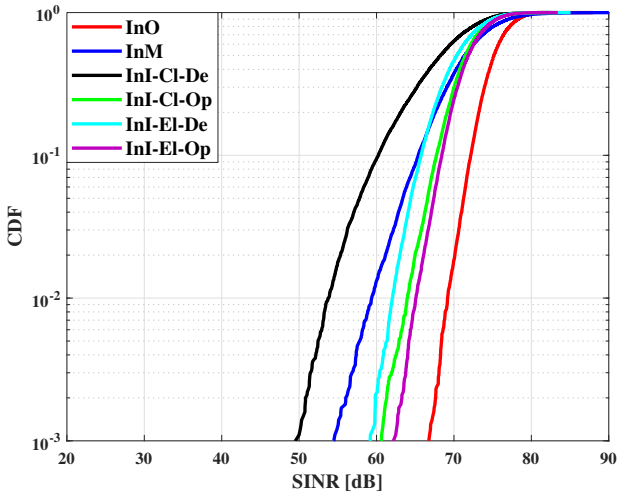

Figure 3: CDF of the SINR when using different channel models with MRT, JT, $J = 16$, and $K = 1$.

C. Deployments comparison

Fig. 4 shows a performance comparison (using the SINR UB) for the following deployments (see Fig. 2, [12]):

1) *Centralized*: A single AP equipped with 64 antennas placed at the center of the factory hall. This case can be seen as a single-cell network;
2) *Partially distributed*: $J = 4$ APs equipped with 16 antennas each. The inter-AP distance (IAD) along the longest side is 50 m while the IAD along the shortest side is 25 m;
3) *Fully distributed*: $J = 16$ APs equipped with 4 antennas each. The IAD along longest side is 25 m while the IAD along shortest side is 12.5 m.

The considered transmission modes are SAT and JT (for the centralized deployment these two transmission modes are equivalent), while the adopted beamformer is the MRT. The results depict that the centralized deployment achieves the worst performance. In particular, in the lower part of the SINR CDF curves, the best performance is attained by the partially distributed deployment, which retains both the benefits of distributed deployment and multiple antenna processing at each AP. Results also show that, as expected, JT provides much better performance than SAT. It should be however noted that the JT scheme is the one with the highest complexity. In the remaining part of this section, we focus the numerical analysis only on the partially distributed deployment ($J = 4$).

D. Comparing UB and LB SINR behaviour

Fig. 5 shows the gap between the Upper Bound and the Lower Bound, in term of SINR and of average rate per user versus error probability, when the MRT beamformer is used, for the JT, CFT and SAT transmission modes. We see that the gap between the bounds is rather limited, and this is of course a positive result since the bounds can be assumed to be representative of the true SINR values with a limited approximation error. The gap in case of JT is a bit larger than that of the other transmission modes, i.e. about 1 dB,

This article has been accepted for publication in a future issue of this journal, but has not been fully edited. Content may change prior to final publication. Citation information: DOI 10.1109/OJCOMS.2021.3089281, IEEE Open Journal of the Communications Society

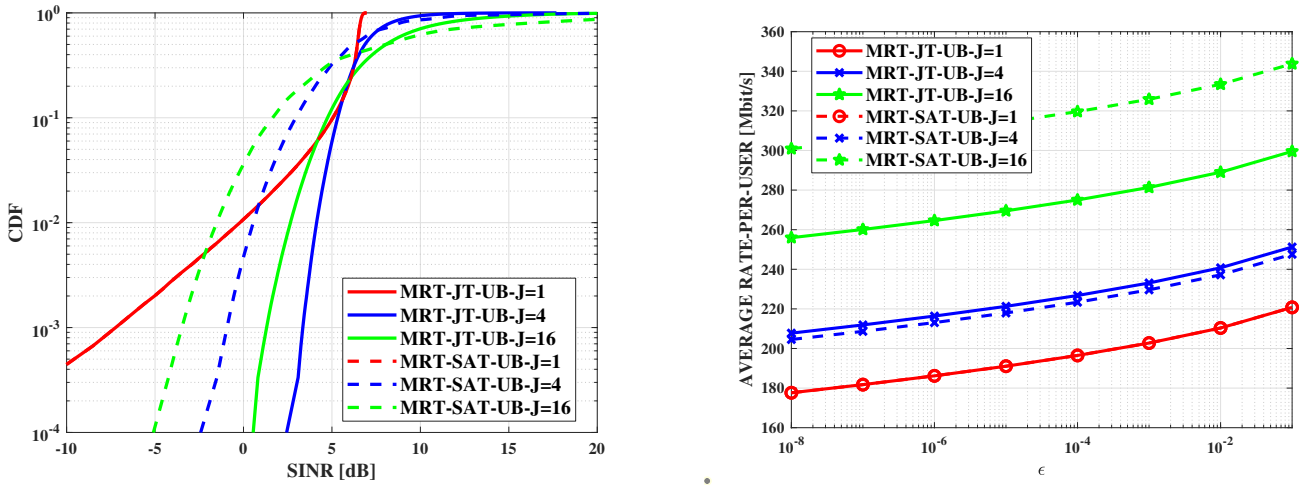

Figure 4: SINR CDF and average rate-per-user with MRT for different transmission modes, JT and SAT, and different deployments.

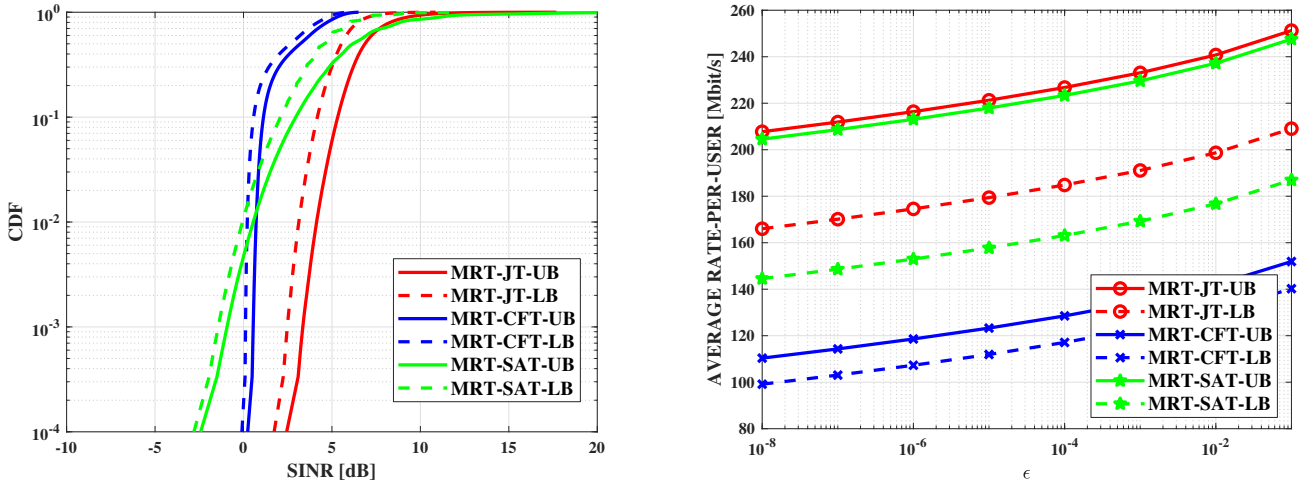

Figure 5: SINR CDF and average rate-per-user with MRT for different transmission modes, JT, CFT, and SAT; comparison between Upper Bound and Lower Bound.

compared to ∼0.5-0.7 dB in case of CFT and SAT, in the low SINR region. Based on the evidence that there is a limited gap between the UB and LB, in the sequel we will report the UB curves only for the sake of clarity and plot readability.

E. Impact of beamformers

Fig. 6 presents the achieved performance when MRT and FZF beamformers are employed, for different transmission modes, i.e. JT, CFT, and SAT. Inspecting the curves, an interesting trade-off emerges. Focusing on the plot of the SINR CDF, it is seen that for JT the ZF strategy is uniformly better than the MRT strategy. Conversely, for CFT and SAT the curves corresponding to ZF and MRT cross at some point. So, as far as reliability is concerned, i.e. in the lower-left part of the curve, MRT achieves better performance than ZF. This may be explained by noticing that SINR for users with weak channels, are mostly affected by noise rather than by interference, and, so they suffer the noise enhancement effect that is produced by the ZF processing. Results also show that in the lower-left part of the curve CFT provides better performance than SAT, while the opposite happens in the upper-right part of the CDF. If we look at the average rates, instead (i.e., the subplot on the right), the ZF has always better performance than the MRT beamformer, and SAT outperforms CFT. Fig. 7 provides a comparison between the ZF beamformer and the PZF (evaluated with $N_j = 7$ and $N_j = 8$), for CFT and SAT. Again, the CDF curves cross at some point. In the lower-left part of the plot, PZF with $N_j = 7$ exhibits the best performance. In terms of mean rates, CFT with PZF and $N_j = 8$ achieves the best performance, with more than 20% gains over the ZF beamformer.

F. Advantages of UCT processing

In Fig. 8 the UC transmission mode is contrasted with CFT. Results clearly show that UC transmission outperforms, both in the lower-left part of the plot reporting the CDF of the SINR, and in terms of mean rates, the other transmission modes. Indeed, UC retains the advantages of distributed antenna transmissions, but, at the same time, avoids the inefficient situation where APs have to waste their energy to

This article has been accepted for publication in a future issue of this journal, but has not been fully edited. Content may change prior to final publication. Citation information: DOI 10.1109/OJCOMS.2021.3089281, IEEE Open Journal of the Communications Society

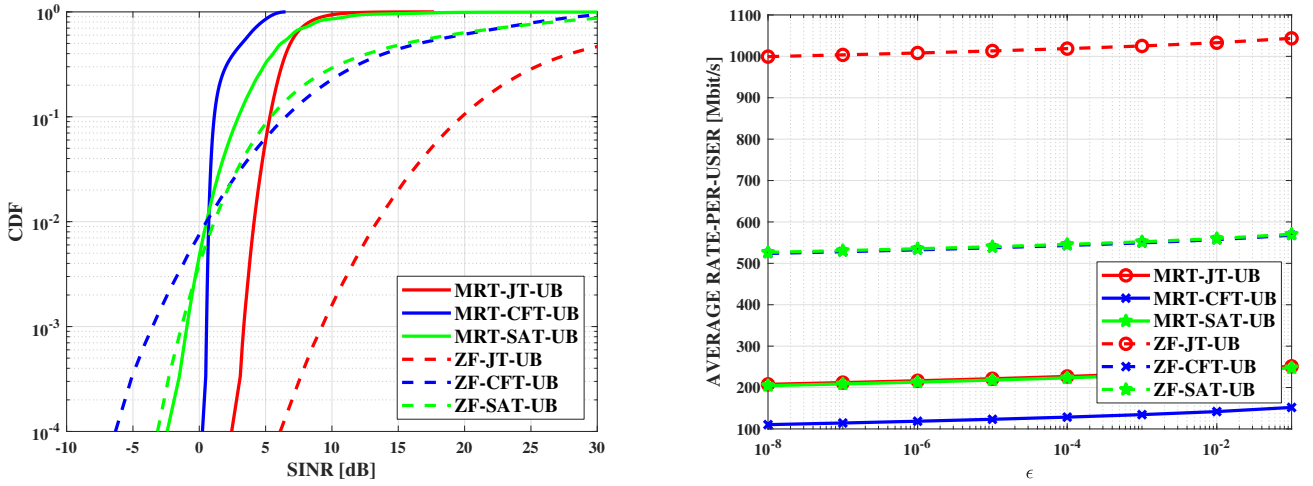

Figure 6: SINR CDF and average rate-per-user with MRT versus FZF for different transmission modes, JT, CFT, and SAT.

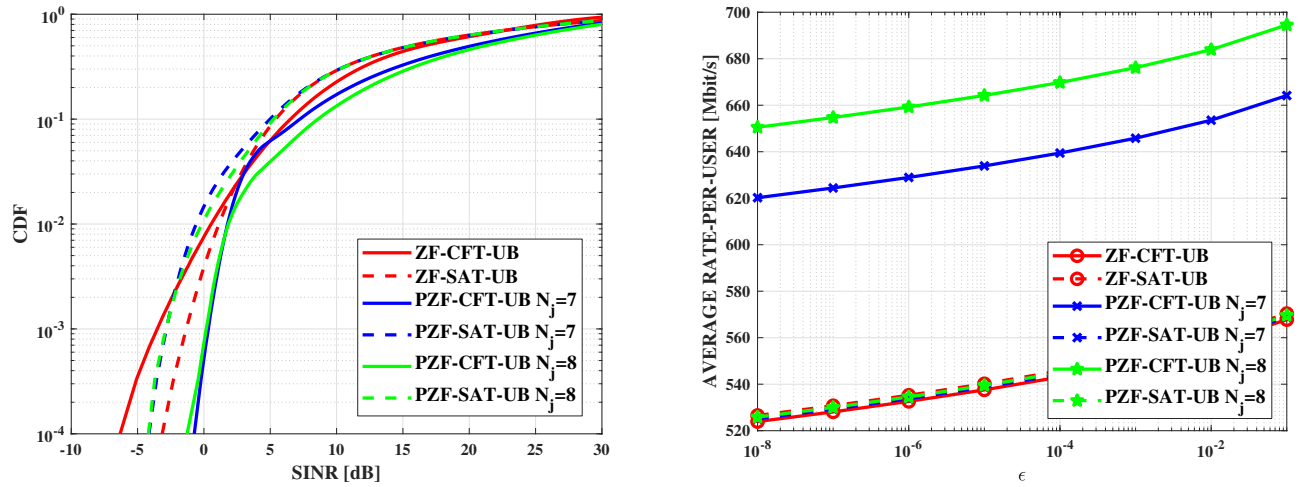

Figure 7: SINR CDF and average rate-per-user with FZF versus PZF with $N_j = 7$ and $N_j = 8$ for different transmission modes, CFT and SAT.

transmit to far users with weak channel coefficients, potentially even creating more interference to the ACs that are close by. Comparing the results in Fig. 8 with those in Fig. 6 it appears that JT outperforms the UC transmission mode, but this was to be expected since JT performs a highly complex joint processing.

G. Impact of power control

In Fig. 9 we finally assess the effect of the power control rule, assuming ZF beamforming, and comparing SAT, JT, CFT and UC mode with $N = 3$. Results show that the power control rule is highly effective in the lower-left part of the CDF of the SINR curve. Again, results confirm that the UCT mode is outperformed by the JT only, while outperforming the SAT and CFT modes.

VII. Conclusions

The paper considered distributed antenna settings in an indoor industrial scenario. Several transmission modes and several beamformers have been adopted, along with a power control rule maximizing the minimum SINR across users, which is extremely useful in industrial settings where reliability is to be privileged with respect to peak data rates. Moreover, the SINR upper bound and lower bound are derived in the paper. Overall, numerical results have shown that the user centric transmission mode, wherein each AC is served by a limited number of APs in the neighbors, and the partially distributed deployment, achieve the best trade-off between implementation complexity and system performance. Current work is focused on the extension of the proposed analysis to the case in which millimeter wave carrier frequencies are adopted.

Appendix

A. Derivation of the SINR Lower Bound for UCT

We have to find a closed form for the terms D_k, B_k, and $I_{k,l}$.

1) Evaluation of D_k

Denoting by $\tilde{\mathbf{h}}_{k,j} = \mathbf{h}_{k,j} - \hat{\mathbf{h}}_{k,j}$ the channel estimation error, and it is known, from the LMMSE estimation, that $\tilde{\mathbf{h}}_{k,j}$ $\hat{\mathbf{h}}_{k,j}$

This article has been accepted for publication in a future issue of this journal, but has not been fully edited. Content may change prior to final publication. Citation information: DOI 10.1109/OJCOMS.2021.3089281, IEEE Open Journal of the Communications Society

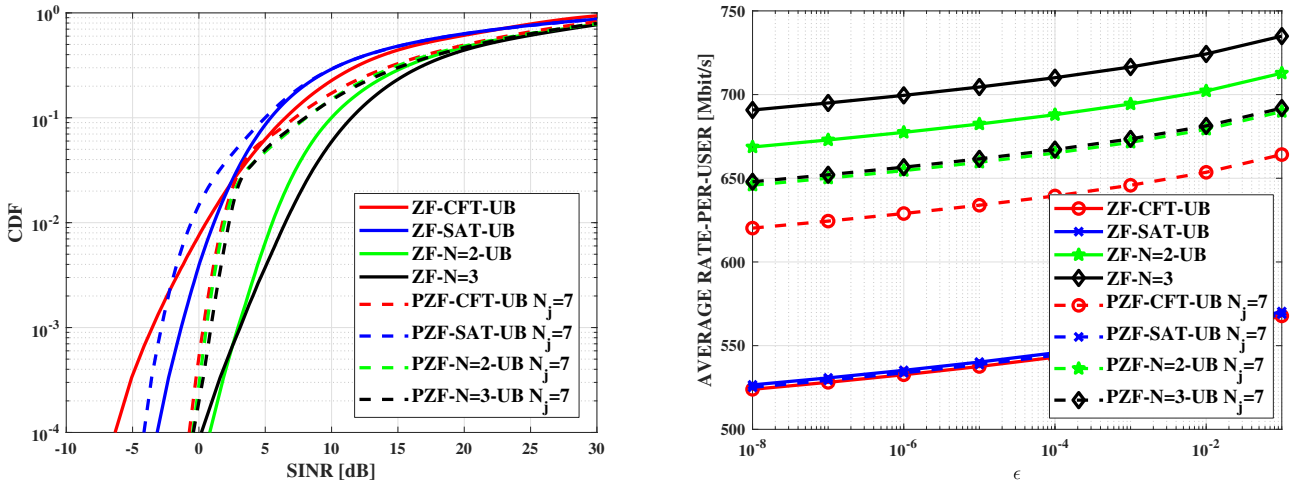

Figure 8: SINR CDF and average rate-per-user with FZF versus PZF with $N_j = 7$ for different transmission modes, CFT, SAT, UC with N=2 and N=3.

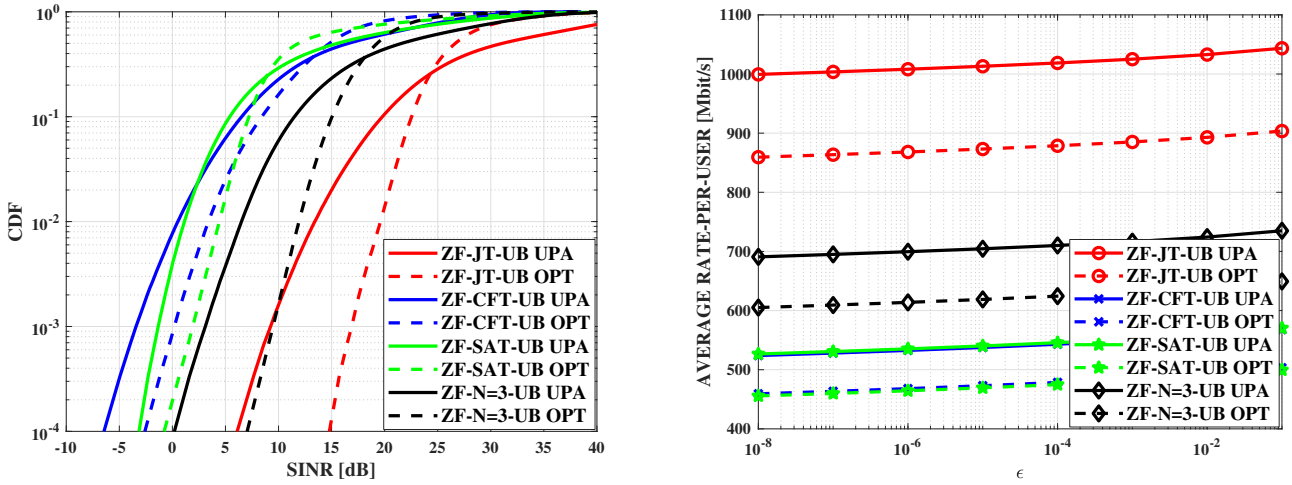

Figure 9: SINR CDF and a verage rate-per-user with FZF with uniform and optimal power allocation, CFT, SAT, UCT with N=3.

are independent. So, by substituting $\mathbf{h}_{k,j} = \tilde{\mathbf{h}}_{k,j} + \hat{\mathbf{h}}_{k,j}$, it is possible to derive the following expression:

$$D_k = \mathbb{E}\left[\sum_{j\in J(k)} \sqrt{\eta_{k,j}}\mathbf{h}_{k,j}^H \hat{\mathbf{h}}_{k,j}\right] = \sum_{j\in J(k)} \sqrt{\eta_{k,j}}\mathbb{E}\left[\mathbf{h}_{k,j}^H \hat{\mathbf{h}}_{k,j}\right] = \sum_{j\in J(k)} \sqrt{\eta_{k,j}}\left(\mathbb{E}\left[\hat{\mathbf{h}}_{k,j}^H \hat{\mathbf{h}}_{k,j}\right] + \mathbb{E}\left[\tilde{\mathbf{h}}_{k,j}^H \hat{\mathbf{h}}_{k,j}\right]\right) = \sum_{j\in J(k)} \sqrt{\eta_{k,j}}\gamma_{k,j} \tag{29}$$

In eq.(29) $\gamma_{k,j}$ is defined as:

$$\gamma_{k,j} = \mathbb{E}\left[\hat{\mathbf{h}}_{k,j}^H \hat{\mathbf{h}}_{k,j}\right] = tr\left(\mathbb{E}\left[\hat{\mathbf{h}}_{k,j}\hat{\mathbf{h}}_{k,j}^H\right]\right) = tr\left(\mathbb{E}\left[\alpha_{k,j}\check{\mathbf{y}}_{k,j}\check{\mathbf{y}}_{k,j}^H\alpha_{k,j}\right]\right) = \sqrt{\eta_k^{UL-T}}\beta_{k,j}\alpha_{k,j}M. \tag{30}$$

2) Evaluation of $\mathbb{E}\left[|B_k|^2\right]$

Since the variance of a sum of independent RVs is equal to the sum of their variances, $\mathbb{E}\left[|B_k|^2\right]$ can be written as:

$$\mathbb{E}\left[|B_k|^2\right] = \mathbb{E}\left[\left|\sum_{j\in J(k)} \sqrt{\eta_{k,j}}\left(\mathbf{h}_{k,j}^H \hat{\mathbf{h}}_{k,j} - \mathbb{E}\left[\mathbf{h}_{k,j}^H \hat{\mathbf{h}}_{k,j}\right]\right)\right|^2\right] = \sum_{j\in J(k)} \eta_{k,j}\mathbb{E}\left[\left|\mathbf{h}_{k,j}^H \hat{\mathbf{h}}_{k,j} - \mathbb{E}\left[\mathbf{h}_{k,j}^H \hat{\mathbf{h}}_{k,j}\right]\right|^2\right] = \sum_{j\in J(k)} \eta_{k,j}\left(\mathbb{E}\left[\left|\mathbf{h}_{k,j}^H \hat{\mathbf{h}}_{k,j}\right|^2\right] - \left|\underbrace{\mathbb{E}\left[\mathbf{h}_{k,j}^H \hat{\mathbf{h}}_{k,j}\right]}_{\gamma_{k,j}}\right|^2\right). \tag{31}$$

Now we can evaluate the term $\mathbb{E}\left[\left|\mathbf{h}_{k,j}^H\hat{\mathbf{h}}_{k,j}\right|^2\right]$:

$$\begin{aligned}
&\mathbb{E}\left[\left|\mathbf{h}_{k,j}^H\hat{\mathbf{h}}_{k,j}\right|^2\right] = \\
&\mathbb{E}\left[\left|\mathbf{h}_{k,j}^H\alpha_{k,j}\left(\sum_{l=1}^{K}\sqrt{\eta_l^{UL-T}}\mathbf{h}_{l,j}\varphi_{l,k}+\tilde{\mathbf{w}}_{k,j}\right)\right|^2\right] = \\
&\alpha_{k,j}^2\eta_k^{UL-T}\mathbb{E}\left[\left|\mathbf{h}_{k,j}^H\mathbf{h}_{k,j}\right|^2\right]+ \\
&\sum_{l=1,l\neq k}^{K}\eta_l^{UL-T}\alpha_{k,j}^2\mathbb{E}\left[\left|\mathbf{h}_{k,j}^H\mathbf{h}_{l,j}\right|^2\right]\left|\varphi_{l,k}\right|^2+ \\
&\alpha_{k,j}^2\mathbb{E}\left[\left|\mathbf{h}_{k,j}^H\tilde{\mathbf{w}}_{k,j}\right|^2\right] = \alpha_{k,j}^2\eta_k^{UL-T}\mathbb{E}\left[\left|\mathbf{h}_{k,j}^H\mathbf{h}_{k,j}\right|^2\right]+ \\
&\sum_{l=1,l\neq k}^{K}\eta_l^{UL-T}\alpha_{k,j}^2\mathbb{E}\left[\mathbf{h}_{k,j}^H\mathbf{h}_{l,j}\mathbf{h}_{l,j}^H\mathbf{h}_{k,j}\right]\left|\varphi_{l,k}\right|^2+ \\
&\alpha_{k,j}^2\mathbb{E}\left[\mathbf{h}_{k,j}^H\tilde{\mathbf{w}}_{k,j}\tilde{\mathbf{w}}_{k,j}^H\mathbf{h}_{k,j}\right] = \\
&= \alpha_{k,j}^2\eta_k^{UL-T}\mathbb{E}\left[\left|\mathbf{h}_{k,j}^H\mathbf{h}_{k,j}\right|^2\right]+ \\
&\sum_{l=1,l\neq k}^{K}\eta_l^{UL-T}\alpha_{k,j}^2\beta_{l,j}\beta_{k,j}M\left|\varphi_{l,k}\right|^2+\alpha_{k,j}^2\beta_{k,j}\sigma_w^2M
\end{aligned} \tag{32}$$

where $\tilde{\mathbf{w}}_{k,j} = \mathbf{W}_j\mathbf{\Phi}_{:,k}$. We have to evaluate the terms $\mathbb{E}\left[\mathbf{h}_{k,j}^H\mathbf{h}_{l,j}\mathbf{h}_{l,j}^H\mathbf{h}_{k,j}\right]$ and $\mathbb{E}\left[\left|\mathbf{h}_{k,j}^H\mathbf{h}_{k,j}\right|\right]$, and they are obtained as follows:

$$\begin{aligned}
&\mathbb{E}\left[\mathbf{h}_{k,j}^H\mathbf{h}_{l,j}\mathbf{h}_{l,j}^H\mathbf{h}_{k,j}\right] = \mathbb{E}\left[tr\left(\mathbf{h}_{l,j}\mathbf{h}_{l,j}^H\mathbf{h}_{k,j}\mathbf{h}_{k,j}^H\right)\right] = \\
&tr\left(\mathbb{E}\left[\mathbf{h}_{l,j}\mathbf{h}_{l,j}^H\mathbf{h}_{k,j}\mathbf{h}_{k,j}^H\right]\right) = \beta_{k,j}\beta_{l,j}M\ ,
\end{aligned} \tag{33}$$

and

$$\begin{aligned}
&\mathbb{E}\left[\left|\mathbf{h}_{k,j}^H\mathbf{h}_{k,j}\right|\right] = \text{tr}^2(\beta_{k,j}\mathbf{I}_M)+\text{tr}(\beta_{k,j}\mathbf{I}_M\beta_{k,j}\mathbf{I}_M) = \\
&\beta_{k,j}^2M^2+\beta_{k,j}^2M = \beta_{k,j}^2(M+1)M
\end{aligned} \tag{34}$$

Substituting Eq. (33) and (34) in Eq. (32) first, and then in Eq. (31) we finally get:

$$\begin{aligned}
&\mathbb{E}\left[|B_k|^2\right] = \sum_{j\in J(k)}\eta_{k,j}\left(\gamma_{k,j}^2+\gamma_{k,j}\beta_{k,j}-\gamma_{k,j}^2\right) = \\
&\sum_{j\in J(k)}\eta_{k,j}\gamma_{k,j}\beta_{k,j}
\end{aligned} \tag{35}$$

3) Evaluation of $\mathbb{E}\left[|I_{k,l}|^2\right]$

As it has been done for $\mathbb{E}\left[|B_k|^2\right]$, it is possible to follows a similar approach.

$$\begin{aligned}
&\mathbb{E}\left[|I_{k,l}|^2\right] = \mathbb{E}\left[\left|\sum_{j\in J(l)}\sqrt{\eta_{l,j}}\mathbf{h}_{k,j}^H\hat{\mathbf{h}}_{l,j}\right|^2\right] = \\
&\mathbb{E}\left[\left|\sum_{j\in J(l)}\sqrt{\eta_{l,j}}\alpha_{l,j}\mathbf{h}_{k,j}^H\left(\sum_{i=1}^{K}\eta_i^{UL-T}\mathbf{h}_{i,j}\varphi_{i,l}+\tilde{\mathbf{W}}_{l,j}\right)\right|^2\right] = \\
&= \mathbb{E}\left[\left|\sum_{j\in J(l)}\sqrt{\eta_{l,j}}\alpha_{l,j}\mathbf{h}_{k,j}^H\eta_k^{UL-T}\mathbf{h}_{k,j}\varphi_{i,l}\right|^2\right]+ \\
&\mathbb{E}\left[\left|\sum_{j\in J(l)}\sqrt{\eta_{l,j}}\alpha_{l,j}\mathbf{h}_{k,j}^H\left(\sum_{i=1,i\neq k}^{K}\sqrt{\eta_i^{UL-T}}\mathbf{h}_{i,j}\varphi_{i,l}\right)\right|^2\right]+ \\
&+\mathbb{E}\left[\left|\sum_{j\in J(l)}\sqrt{\eta_{l,j}}\alpha_{l,j}\mathbf{h}_{k,j}^H\tilde{\mathbf{W}}_{l,j}\right|^2\right] = \\
&\eta_k^{UL-T}\mathbb{E}\left[\left|\sum_{j\in J(l)}\sqrt{\eta_{l,j}}\alpha_{l,j}\mathbf{h}_{k,j}\mathbf{h}_{k,j}\right|^2\right]\left|\varphi_{k,l}\right|^2+ \\
&+\sum_{j\in J(l)}\sum_{i=1,i\neq k}^{K}\eta_{l,j}\eta_i^{UL-T}\alpha_{l,j}^2\mathbb{E}\left[\left|\mathbf{h}_{k,j}^H\mathbf{h}_{i,j}\right|^2\right]\left|\varphi_{i,l}\right|^2+ \\
&\sum_{j\in J(l)}\eta_{l,j}\alpha_{l,j}^2\mathbb{E}\left[\left|\mathbf{h}_{k,j}^H\tilde{\mathbf{W}}_{l,j}\right|^2\right] = \\
&= \eta_k^{UL-T}\mathbb{E}\left[\left|\sum_{j\in J(l)}\sqrt{\eta_{l,j}}\alpha_{l,k}\mathbf{h}_{k,j}^H\mathbf{h}_{k,j}\right|^2\right]\left|\varphi_{k,l}\right|^2+ \\
&\sum_{j\in J(l)}\sum_{i=1,i\neq k}^{K}\eta_{l,j}\eta_i^{UL-T}\alpha_{l,j}^2\beta_{i,j}\beta_{k,j}M\left|\varphi_{k,l}\right|^2+ \\
&\sum_{j\in J(l)}\eta_{l,j}\alpha_{l,j}^2\beta_{k,j}\sigma_w^2M
\end{aligned} \tag{36}$$

At this point, $\mathbb{E}\left[\left|\sum_{j\in J(l)}\sqrt{\eta_{l,j}}\alpha_{l,k}\mathbf{h}_{k,j}^H\mathbf{h}_{k,j}\right|^2\right]$ has to be evaluated:

$$\begin{aligned}
&\mathbb{E}\left[\left|\sum_{j\in J(l)}\sqrt{\eta_{l,j}}\alpha_{l,j}\mathbf{h}_{k,j}^H\mathbf{h}_{k,j}\right|^2\right] = \\
&\mathbb{E}\left[\left(\sum_{j\in J(l)}\sqrt{\eta_{l,j}}\alpha_{l,j}^2\mathbf{h}_{k,j}^H\mathbf{h}_{k,j}\right)\left(\sum_{j'\in J(l)}\sqrt{\eta_{l,j'}}\alpha_{l,j'}\mathbf{h}_{k,j'}^H\mathbf{h}_{k,j'}\right)\right] = \\
&\sum_{j\in J(l)}\eta_{l,j}\alpha_{l,j}^2\left(\beta_{k,j}^2M^2+\beta_{k,j}^2M\right)+ \\
&\sum_{j\in J(l)}\sum_{j'\in J(l),j'\neq j}\sqrt{\eta_{l,j}}\sqrt{\eta_{l,j'}}\alpha_{l,j}\alpha_{l,j'}\beta_{k,j}\beta_{k,j'}M^2 = \\
&= \sum_{j\in J(l)}\eta_{l,j}\alpha_{l,j}^2\beta_{k,j}^2M+\left(\sum_{j\in J(l)}\sqrt{\eta_{l,j}}\alpha_{l,j}\beta_{k,j}M\right)^2
\end{aligned} \tag{37}$$

Substituting, now, Eq. (37) in Eq. (36) we get:

$$\mathbb{E}\left[|I_{k,l}|^2\right] = \eta_k^{UL-T} \times \left[\sum_{j\in J(l)} \eta_{l,j}\alpha_{l,j}^2\beta_{k,j}^2 M + \left(\sum_{j\in J(l)} \sqrt{\eta_{l,j}}\alpha_{l,j}\beta_{k,j}M\right)^2\right]\left|\varphi_{k,l}\right|^2 + + \sum_{j\in J(l)}\sum_{i=1,i\neq k}^{K} \eta_{l,j}\eta_i^{UL-T}\alpha_{l,j}^2\beta_{i,j}\beta_{k,j}M\left|\varphi_{i,l}\right|^2 + \sum_{j\in J(l)} \eta_{l,j}\alpha_{l,j}^2\beta_{k,j}\sigma_w^2 M = = \sum_{j\in J(l)} \sqrt{\eta_{l,j}}\alpha_{l,j}^2\beta_{k,j}M \underbrace{\left(\sum_{i=1}^{K}\eta_i^{UL-T}\beta_{i,j}\left|\varphi_{i,l}\right| + \sigma_w^2\right)}_{\text{den}(\alpha_{l,j})} + \left(\sum_{j\in J(l)}\sqrt{\eta_k^{UL-T}}\sqrt{\eta_{l,j}}\alpha_{l,j}\beta_{k,j}M\right)^2\left|\varphi_{k,l}\right|^2 = = \sum_{j\in J(l)} \eta_{l,j}\beta_{k,j}\frac{\overbrace{\sqrt{\eta_l^{UL-T}}\alpha_{l,j}\beta_{l,j}M}^{\gamma_{l,j}}}{\text{den}(\alpha_{l,j})}\text{den}(\alpha_{l,j}) + \left(\sum_{j\in J(l)}\sqrt{\eta_{l,j}}\alpha_{l,j}\beta_{k,j}M\right)^2\left|\varphi_{k,l}\right|^2 = \sum_{j\in J(l)}\eta_{l,j}\beta_{k,j}\alpha_{l,j} + \left(\sum_{j\in J(l)}\sqrt{\eta_{l,j}}\frac{\sqrt{\eta_k^{UL-T}}}{\sqrt{\eta_k^{UL-T}}}\frac{\beta_{k,j}}{\beta_{l,j}}\alpha_{l,j}\right)^2\left|\varphi_{k,l}\right|^2 \tag{38}$$

where $\text{den}(\alpha_{k,j})$ is the denominator of $\alpha_{k,j}$ defined in Eq. (5). Finally, we can plug Eq. (29), Eq. (35) and Eq.(38) into Eq. (12) to obtain Eq. (13).

B. Derivation of the SINR Lower Bound for JT

1) Definition of block matrices

It is possible to write $\hat{\mathbf{h}}_k = \mathbf{D}_k\check{\mathbf{y}}_k$, where $\mathbf{D}_k$ is a $(M_{TOT}\times M_{TOT})$ block diagonal matrix defined in Section IV and $\check{\mathbf{y}}_k$ is defined as:

$$\check{\mathbf{y}}_k = \begin{bmatrix} \check{\mathbf{y}}_{k,1} \\ \check{\mathbf{y}}_{k,2} \\ \vdots \\ \check{\mathbf{y}}_{k,J} \end{bmatrix} \tag{39}$$

So we have the following power constraint: $\eta_k\mathbb{E}\left[\hat{\mathbf{h}}_k^H\hat{\mathbf{h}}_k\right] \leq P_{max}$. We know that $\mathbb{E}\left[\hat{\mathbf{h}}_k^H\hat{\mathbf{h}}_k\right] = \text{tr}\left(\mathbb{E}\left[\hat{\mathbf{h}}_k\hat{\mathbf{h}}_k^H\right]\right)$ so we can write $\mathbb{E}\left[\hat{\mathbf{h}}_k\hat{\mathbf{h}}_k^H\right] = \mathbb{E}\left[\mathbf{D}_k\check{\mathbf{y}}_k\check{\mathbf{y}}_k^H\mathbf{D}_k^H\right]$.

2) Evaluation of $\mathbb{E}\left[\check{\mathbf{y}}_k\check{\mathbf{y}}_k^H\right]$

: it is possible to evaluate separately the quantity $\mathbb{E}\left[\check{\mathbf{y}}_k\check{\mathbf{y}}_k^H\right]$, so first of all we define:

$$\check{\mathbf{y}}_{k,j} = \sqrt{\eta_k^{UL-T}}\mathbf{h}_{k,j} + \sum_{l\neq k}\sqrt{\eta_l^{UL-T}}\mathbf{h}_{l,j}\varphi_{l,k} + \tilde{\mathbf{W}}_{k,j}, \tag{40}$$

then,

$$\mathbb{E}\left[\check{\mathbf{y}}_{k,j}\check{\mathbf{y}}_{k,j}^H\right] = \left(\sum_{l=1}^{K}\eta_l^{UL-T}\beta_{l,j}\left|\varphi_{l,k}\right|^2 + \sigma_w^2\right)\mathbf{I}_M = c_{k,j}\mathbf{I}_M. \tag{41}$$

Now, assuming that the channels among users and APs are independent:

$$\mathbb{E}\left[\check{\mathbf{y}}_k\check{\mathbf{y}}_k^H\right] = \mathbf{C}_k = \begin{bmatrix} c_{k,1}\mathbf{I}_M & 0 & \dots & 0 \\ 0 & c_{k,2}\mathbf{I}_M & \dots & 0 \\ \vdots & \vdots & \ddots & \vdots \\ 0 & 0 & \dots & c_{k,J}\mathbf{I}_M \end{bmatrix} \tag{42}$$

Since $\alpha_{k,j} = \frac{\sqrt{\eta_k^{UL-T}}\beta_{k,j}}{c_{k,j}}$ and we are dealing with diagonal matrices we can rewrite, $\mathbf{D}_k = \sqrt{\eta_k^{UL-T}}\mathbf{B}_k\mathbf{C}_k^{-1}$, where $\mathbf{B}_k$ is defined in Section IV.

In the end, $\sqrt{\eta_k^{UL-T}}\hat{\mathbf{h}}_k = \mathbf{B}_k\mathbf{C}_k^{-1}\check{\mathbf{y}}_k$ and so:

$$\mathbb{E}\left[\hat{\mathbf{h}}_k^H\hat{\mathbf{h}}_k\right] = \mathbf{B}_k\mathbf{C}_k^{-1}\mathbb{E}\left[\check{\mathbf{y}}_{k,j}\check{\mathbf{y}}_{k,j}^H\right]\mathbf{C}_k^{-1}\mathbf{B}_k^H = \sqrt{\eta_k^{UL-T}}\mathbf{D}_k\mathbf{B}_k^H. \tag{43}$$

3) Evaluation of D_k

by looking at the eq.(16) D_k can be written as:

$$D_k = \mathbb{E}\left[\mathbf{h}_k^H\hat{\mathbf{q}}_k\right] = \mathbb{E}\left[\mathbf{h}_k^H\hat{\mathbf{h}}_k\right] = \mathbb{E}\left[\mathbf{h}_k^H\mathbf{D}_k\check{\mathbf{y}}_k\right] = \text{tr}\left(\mathbb{E}\left[\check{\mathbf{y}}_k\mathbf{h}_k^H\right]\mathbf{D}_k\right) = \text{tr}\left(\mathbb{E}\left[\left(\sum_{l=1}^{K}\sqrt{\eta_l^{UL-T}}\mathbf{h}_{l,j}\varphi_{l,k} + \tilde{\mathbf{W}}_{k,j}\right)\mathbf{h}_k^H\right]\mathbf{D}_k\right) = = \text{tr}\left(\sqrt{\eta_k^{UL-T}}\mathbb{E}\left[\mathbf{h}_k\mathbf{h}_k^H\right]\mathbf{D}_k\right) = \gamma_k \tag{44}$$

4) Evaluation of $\mathbb{E}\left[|B_k|^2\right]$

now, we have to evaluate $\mathbb{E}\left[|B_k|^2\right]$.

$$\mathbb{E}\left[|B_k|^2\right] = \mathbb{E}\left[\left|\mathbf{h}_k^H\mathbf{q}_k - \mathbb{E}\left[\mathbf{h}_k^H\mathbf{q}_k\right]\right|^2\right] = \mathbb{E}\left[\left|\mathbf{h}_k^H\hat{\mathbf{h}}_k\right|^2\right] - \left|\underbrace{\mathbb{E}\left[\mathbf{h}_k^H\hat{\mathbf{h}}_k\right]}_{\gamma_k}\right|^2 \tag{45}$$

Assuming that all the channels are independent it is possible to follow the same approach for the UC; then we can write:

$$\mathbb{E}\left[|B_k|^2\right] = \sqrt{\eta_k^{UL-T}}\text{tr}(\mathbf{B}_k\mathbf{D}_k^H\mathbf{B}_k). \tag{46}$$

5) Evaluation of $\mathbb{E}\left[\left|I_{k,l}\right|^2\right]$

From eq.(16) we have to evaluate $\mathbb{E}\left[\left|\mathbf{h}_k^H\hat{\mathbf{h}}_l\right|^2\right]$:

$$\mathbb{E}\left[\left|I_{k,l}\right|^2\right] = \mathbb{E}\left[\left|\mathbf{h}_k^H\hat{\mathbf{h}}_l\right|^2\right] = \mathbb{E}\left[\left|\mathbf{h}_k^H\mathbf{D}_l\check{\mathbf{y}}_l\right|^2\right] =$$
$$\mathbb{E}\left[\left|\mathbf{h}_k^H\mathbf{D}_l(\sum_{i=1}^{K}\sqrt{\eta_i^{UL-T}}\mathbf{h}_{i,j}\mathbf{\Phi}_{:,i}^H\mathbf{\Phi}_{:,k}+\tilde{\mathbf{W}}_l)\right|^2\right] =$$
$$=$$
$$\eta_k^{UL-T}\left[\mathrm{tr}^2\left(\mathbf{D}_l\mathbf{B}_k\right)+\mathrm{tr}\left(\mathbf{D}_l\mathbf{B}_k\mathbf{D}_l^H\mathbf{B}_k\right)\right]\left|\varphi_{k,l}\right|^2 +$$
$$+\sum_{i=1,i\neq k}^{K}\eta_i^{UL-T}\mathrm{tr}\left(\mathbf{D}_l\mathbf{B}_i\mathbf{D}_l^H\mathbf{B}_k\right)\left|\varphi_{i,l}\right|^2+\sigma_w^2\mathrm{tr}\left(\mathbf{D}_l\mathbf{D}_l^H\mathbf{B}_k\right) =$$
$$\eta_k^{UL-T}\mathrm{tr}^2\left(\mathbf{D}_l\mathbf{B}_k\right)\left|\varphi_{k,l}\right|^2 +$$
$$\sum_{i=1}^{K}\eta_i^{UL-T}\mathrm{tr}\left(\mathbf{D}_l\mathbf{B}_i\mathbf{D}_l^H\mathbf{B}_k\right)\left|\varphi_{i,l}\right|^2+\sigma_w^2\mathrm{tr}\left(\mathbf{D}_l\mathbf{D}_l^H\mathbf{B}_k\right)\overset{(a)}{=}$$
$$\eta_k^{UL-T}\mathrm{tr}^2\left(\mathbf{D}_l\mathbf{B}_k\right)\left|\varphi_{k,l}\right|^2 +$$
$$\mathrm{tr}\Bigg[\mathbf{D}_l\Bigg(\underbrace{\sum_{i=1}^{K}\eta_i^{UL-T}\mathbf{B}_i\left|\varphi_{i,l}\right|^2+\sigma_w^2\mathbf{I}_{M_{TOT}}}_{\mathbf{C}_l}\Bigg)\mathbf{D}_l^H\mathbf{B}_k\Bigg] =$$
$$=\eta_k^{UL-T}\mathrm{tr}^2\left(\mathbf{D}_l\mathbf{B}_k\right)\left|\varphi_{k,l}\right|^2+\mathrm{tr}\left(\mathbf{D}_l\mathbf{C}_l\mathbf{D}_l^H\mathbf{B}_k\right)\overset{(b)}{=}$$
$$\overset{(b)}{=}\eta_k^{UL-T}\mathrm{tr}^2\left(\mathbf{D}_l\mathbf{B}_k\right)\left|\varphi_{k,l}\right|^2+\sqrt{\eta_l^{UL-T}}\mathrm{tr}\left(\mathbf{B}_l\mathbf{D}_l^H\mathbf{B}_k\right) \tag{47}$$

where in (a) we exploited the linearity of the trace and in (b) we exploited $\mathbf{D}_l=\sqrt{\eta_l^{UL-T}}\mathbf{B}_l\mathbf{C}_l^{-1}$. In the end, summing up all the terms in the eq.(44),(46),(47) we get eq.(18).

REFERENCES

[1] M. Wollschlaeger, T. Sauter, and J. Jasperneite, "The future of industrial communication: Automation networks in the era of the internet of things and Industry 4.0," *IEEE Industrial Electronics Magazine*, vol. 11, no. 1, pp. 17–27, Mar. 2017.

[2] B. Holfeld, D. Wieruch, T. Wirth, L. Thiele, S. A. Ashraf, J. Huschke, I. Aktas, and J. Ansari, "Wireless communication for factory automation: an opportunity for LTE and 5G systems," *IEEE Communications Magazine*, vol. 54, no. 6, pp. 36–43, Jun. 2016.

[3] M. Gidlund, T. Lennvall, and J. Åkerberg, "Will 5G become yet another wireless technology for industrial automation?" in *2017 IEEE International Conference on Industrial Technology (ICIT)*, Mar. 2017, pp. 1319–1324.

[4] C. Stefanović, "Industry 4.0 from 5G perspective: Use-cases, requirements, challenges and approaches," in *2018 11th CMI International Conference: Prospects and Challenges Towards Developing a Digital Economy within the EU*, Nov. 2018, pp. 44–48.

[5] M. Bennis, M. Debbah, and H. V. Poor, "Ultrareliable and low-latency wireless communication: Tail, risk, and scale," *Proceedings of the IEEE*, vol. 106, no. 10, pp. 1834–1853, Oct. 2018.

[6] H. Chen, R. Abbas, P. Cheng, M. Shirvanimoghaddam, W. Hardjawana, W. Bao, Y. Li, and B. Vucetic, "Ultra-reliable low latency cellular networks: Use cases, challenges and approaches," *IEEE Communications Magazine*, vol. 56, no. 12, pp. 119–125, Dec. 2018.

[7] 3rd Generation Partnership Project (3GPP), "Service requirements for the 5G system," Tech. Rep., TS 22.261, Sep. 2018.

[8] O. N. C. Yilmaz, Y. P. E. Wang, N. A. Johansson, N. Brahmi, S. A. Ashraf, and J. Sachs, "Analysis of ultra-reliable and low-latency 5G communication for a factory automation use case," in *2015 IEEE International Conference on Communication Workshop (ICCW)*, Jun. 2015, pp. 1190–1195.

[9] A. E. Kalør, R. Guillaume, J. J. Nielsen, A. Mueller, and P. Popovski, "Network slicing for ultra-reliable low latency communication in industry 4.0 scenarios," *arXiv preprint arXiv:1708.09132*, 2017.

[10] X. Jiang, Z. Pang, M. Zhan, D. Dzung, M. Luvisotto, and C. Fischione, "Packet detection by a single OFDM symbol in URLLC for critical industrial control: A realistic study," *IEEE Journal on Selected Areas in Communications*, vol. 37, no. 4, pp. 933–946, Apr. 2019.

[11] H. Ren, C. Pan, Y. Deng, M. Elkashlan, and A. Nallanathan, "Joint power and blocklength optimization for URLLC in a factory automation scenario," *IEEE Transactions on Wireless Communications*, vol. 19, no. 3, pp. 1786–1801, Mar. 2020.

[12] G. Casciano, P. Baracca, and S. Buzzi, "Enabling ultra reliable wireless communications for factory automation with distributed MIMO," in *2019 IEEE Vehicular Technology Conference (VTC-Fall)*, Sep. 2019, pp. 1–7.

[13] R1-1813177, "Scenarios, frequencies and new field measurement results from two operational factory halls at 3.5 GHz for various antenna configurations," Nokia, Tech. Rep., Nov. 2018.

[14] W. Yang and G. Xu, "Optimal downlink power assignment for smart antenna systems," in *1998 IEEE International Conference on Acoustics, Speech and Signal Processing (ICASSP)*, May 1998, pp. 3337–3340.

[15] M. Alonzo, P. Baracca, S. R. Khosravirad, and S. Buzzi, "URLLC for factory automation: an extensive throughput-reliability analysis of D-MIMO," in *WSA 2020; 24th International ITG Workshop on Smart Antennas*, Feb. 2020, pp. 1–6.

[16] 3rd Generation Partnership Project (3GPP), "Study on channel model for frequencies from 0.5 to 100 GHz," Tech. Rep., TR 38.901, Jun. 2018.

[17] H. Q. Ngo, A. Ashikhmin, H. Yang, E. G. Larsson, and T. L. Marzetta, "Cell-free massive MIMO versus small cells," *IEEE Transactions on Wireless Communications*, vol. 16, no. 3, pp. 1834–1850, Mar. 2017.

[18] M. Alonzo and S. Buzzi, "Cell-free and user-centric massive MIMO at millimeter wave frequencies," in *2017 IEEE International Symposium on Personal, Indoor, and Mobile Radio Communications (PIMRC)*, Oct. 2017, pp. 1–5.

[19] Y. Polyanskiy, H. V. Poor, and S. Verdú, "Channel coding rate in the finite blocklength regime," *IEEE Transactions on Information Theory*, vol. 56, no. 5, pp. pp. 2307–2359, May 2010.

[20] H. Q. Ngo, A. Ashikhmin, H. Yang, E. G. Larsson, and T. L. Marzetta, "Cell-free massive MIMO: Uniformly great service for everyone," in *2015 IEEE 16th international workshop on signal processing advances in wireless communications (SPAWC)*, Jun. 2015, pp. 201–205.

[21] S. Buzzi and C. D'Andrea, "Cell-free massive MIMO: User-centric approach," *IEEE Wireless Communications Letters*, vol. 6, no. 6, pp. 706–709, Dec. 2017.

[22] S. Verdu, *Multiuser detection*. Cambridge university press, 1998.

[23] T. L. Marzetta, E. G. Larsson, H. Yang, and H. Q. Ngo, *Fundamentals of Massive MIMO*. Cambridge University Press, 2016.

[24] G. Interdonato, H. Q. Ngo, and E. G. Larsson, "Enhanced normalized conjugate beamforming for cell-free massive MIMO," *IEEE Transactions on Communications*, 2021.

[25] G. Femenias, F. Riera-Palou, A. Álvarez Polegre, and A. García-Armada, "Short-term power constrained cell-free massive-mimo over spatially correlated ricean fading," *IEEE Transactions on Vehicular Technology*, vol. 69, no. 12, pp. 15 200–15 215, 2020.

[26] T. Van Chien, E. Björnson, and E. G. Larsson, "Joint power allocation and load balancing optimization for energy-efficient cell-free massive MIMO networks," *IEEE Transactions on Wireless Communications*, vol. 19, no. 10, pp. 6798–6812, 2020.

[27] S. Boyd and L. Vandenberghe, *Convex optimization*. Cambridge university press, 2004.